

Evolution of level density step structures from $^{56,57}\text{Fe}$ to $^{96,97}\text{Mo}$

A. Schiller,^{1*} E. Tavukcu,^{1,2,3†} L.A. Bernstein,¹ P.E. Garrett,¹ M. Guttormsen,⁴ M. Hjorth-Jensen,⁴
C.W. Johnson,⁵ G.E. Mitchell,^{2,3} J. Rekstad,⁴ S. Siem,⁴ A. Voinov,⁶ W. Younes¹

¹ Lawrence Livermore National Laboratory, L-414, 7000 East Avenue, Livermore, California 94551, USA

² North Carolina State University, Raleigh, North Carolina 27695, USA

³ Triangle Universities Nuclear Laboratory, Durham, North Carolina 27708, USA

⁴ Department of Physics, University of Oslo, N-0316 Oslo, Norway

⁵ San Diego State University, San Diego, California 92182, USA

⁶ Frank Laboratory of Neutron Physics, Joint Institute of Nuclear Research, 141980 Dubna, Moscow region, Russia

Level densities have been extracted from primary γ spectra for $^{56,57}\text{Fe}$ and $^{96,97}\text{Mo}$ nuclei using ($^3\text{He},\alpha\gamma$) and ($^3\text{He},^3\text{He}'\gamma$) reactions on ^{57}Fe and ^{97}Mo targets. The level density curves reveal step structures above the pairing gap due to the breaking of nucleon Cooper pairs. The location of the step structures in energy and their shapes arise from the interplay between single-particle energies and seniority-conserving and seniority-non-conserving interactions.

PACS number(s): 21.10.Ma, 25.55.Hp, 27.40.+z, 27.60.+j

The group at the Oslo Cyclotron Laboratory (OCL) has recently developed a new method (the so-called Oslo method) to extract the level density and radiative strength function from primary γ spectra [1]. The method can be characterized as a further development of the sequential extraction method [2,3]. The Oslo method has been extensively tested in the rare-earth mass region [4–7] and has been successfully extended to the very light $^{27,28}\text{Si}$ nuclei [8]. The robustness of the Oslo method in the mid sd shell where the level density is rather low and the single-particle levels are widely spaced prompted the present investigations in mass regions around the $f_{7/2}$ shell (the iron nuclei) and around the fp_g shell (the molybdenum nuclei). The ^{56}Fe nucleus was especially chosen due to astrophysical interest in this isotope. While Ref. [9] discusses the e -process and the direct production of ^{56}Fe , a modern view in terms of a hierarchy of restricted nuclear statistical equilibria (NSE) on different time scales predicts the direct production of ^{56}Fe only on the highest level of NSE, namely in the presence of weak equilibrium [10]. These rather extreme conditions are envisioned only in the core of massive stars (where ejection into space is unlikely) and in the core of Type Ia supernovae (where ejection into space seems possible). In the equations of NSE, the nuclear partition function, i.e., the Laplace transform of the nuclear level density, plays a prominent role. The nucleus ^{96}Mo is of special interest in the investigation of the $|N - Z|$ dependence of level densities, since the mass 96 isobars are the only ones in the nuclear chart where one can find three different stable nuclei with $|N - Z|$ varying by eight units from ^{96}Zr to ^{96}Ru . Also the $|N - Z|$ dependence of level densities can have significant astrophysical importance [11],

since many reactions take place on unstable isotopes and therefore most of their reaction cross sections must be estimated by Hauser-Feshbach type calculations [12].

The purpose of this Rapid Communication is to report on experimental level densities of $^{56,57}\text{Fe}$ and $^{96,97}\text{Mo}$ nuclei and to provide a schematic explanation of the observed step structures in these curves.

The experiments were performed at the MC-35 cyclotron at the OCL using a ~ 2 nA beam of 45 MeV ^3He particles. The self-supporting targets were isotopically enriched to 94.7% and 94.2% and had thicknesses of 3.4 mg/cm² and 2.1 mg/cm² for ^{57}Fe and ^{97}Mo , respectively. Each experiment ran for approximately five days each, and about 200,000 relevant particle- γ coincidences were recorded in each analyzed reaction channel. The charged ejectiles were identified and their energies measured in a ring of eight collimated Si ΔE - E telescopes placed at 45° with respect to the beam direction. The thicknesses of the front and end detectors were 140 and 3000 μm , respectively and shielding against δ electrons was achieved with a 19- μm -thick Al foil. The distance from the target was 5 cm, giving a total solid angle coverage of 0.3% of 4π , and the energy resolution was ~ 0.3 MeV over the entire spectrum. The γ -rays were detected in 28 collimated 5" x 5" NaI(Tl) detectors called CACTUS [13] surrounding the target and particle detectors. The total efficiency of CACTUS was $\sim 15\%$ of 4π and the resolution was $\sim 6\%$ of the deposited energy at 1.3 MeV. In addition, one 60% Ge(HP) detector was used in the setup to monitor the selectivity and populated spin distribution of the reactions. Raw α -particle data are shown in Fig. 1 for the case of the $^{97}\text{Mo}(^3\text{He},\alpha)^{96}\text{Mo}$ reaction, where discrete transfer peaks are observed up to ~ 6 MeV in excitation energy indicating the opening

*Electronic address: Andreas.Schiller@llnl.gov

†Present address: Osmangazi University, Dept. of Physics, Meselik, Eskisehir, 26480 Turkey

of the neutron $g_{9/2}$ shell.

From the known Q -value and the reaction kinematics, the ejectile energy can be transformed into initial excitation energy of the residual nuclei. Using the particle- γ coincidence technique, each γ ray can be assigned to a cascade depopulating a certain initial excitation energy in the residual nucleus. The data are therefore sorted into total γ -ray spectra originating from different initial excitation energy bins. Every spectrum is then unfolded using a Compton-subtraction method which preserves the fluctuations in the original spectra and does not introduce further, spurious fluctuations [15]. From the unfolded spectra, a primary γ matrix is constructed using the subtraction method of Ref. [16]. The basic assumption behind this method is that the γ -ray decay pattern from any excitation energy bin is independent of whether states in this bin are populated directly via the $({}^3\text{He},\alpha)$ or $({}^3\text{He},{}^3\text{He}')$ reactions or indirectly via γ decay from higher excited levels following the initial nuclear reaction. This assumption is trivially fulfilled if one populates the same levels with the same weights within any excitation energy bin, since the decay branchings are properties of the levels and do not depend on the population mechanisms. On the other hand, if one populates, e.g., vastly different spin distributions within one excitation energy bin via the two different population mechanisms, the γ -decay patterns should be different as well. As an example of the data analysis discussed in this paragraph, the raw, unfolded and primary γ spectra are shown for the ${}^{57}\text{Fe}({}^3\text{He},\alpha\gamma){}^{56}\text{Fe}$ and ${}^{57}\text{Fe}({}^3\text{He},{}^3\text{He}'\gamma){}^{57}\text{Fe}$ reactions in Fig. 2.

Finally, the primary γ matrix is factorized using the generalized Brink-Axel hypothesis [17,18]. The original hypothesis states that the giant dipole resonance (GDR) can be built on every excited state, and that the properties of the GDR do not depend on the temperature of the nuclear state on which it is built. This hypothesis can be generalized to include not only the GDR but any type of nuclear excitation and results in the assumption that primary γ spectra originating from the excitation energy E can be factorized into a γ -ray transmission coefficient $\mathcal{T}(E_\gamma)$ which depends only on the γ -transition energy E_γ and into the level density $\rho(E - E_\gamma)$ at the final energy. This factorization is determined by a least χ^2 fit to the primary γ matrix, using no *a priori* assumptions about the functional form of either the level density or the γ -ray transmission coefficient [1]. An example to illustrate the quality of the fit is shown in Fig. 3, where for the ${}^{97}\text{Mo}({}^3\text{He},{}^3\text{He}'\gamma){}^{97}\text{Mo}$ reaction we compare the experimental primary γ spectra from two different initial excitation energies to the least χ^2 fit. Unfortunately, the mathematical structure of the relevant equations in the least χ^2 fit does not allow us to find a unique solution for the level density and γ -ray transmission coefficient. However, it has been shown that all solutions with the same χ^2 can be obtained by the transformation of one randomly chosen solution according to [1]

$$\tilde{\rho}(E - E_\gamma) = A \exp[\alpha(E - E_\gamma)]\rho(E - E_\gamma) \quad (1)$$

$$\tilde{\mathcal{T}}(E_\gamma) = B \exp(\alpha E_\gamma)\mathcal{T}(E_\gamma). \quad (2)$$

The three free parameters A , B , and α have to be determined to give the physically most relevant solution to the least χ^2 fit using independent experimental information. The most common way is to count the number of discrete levels at low excitation energies and to use the neutron resonance spacing at B_n to find values for A and α . The remaining parameter B is then determined using the average total radiative width of neutron resonances [6]. Unfortunately, in the case of ${}^{56}\text{Fe}$, there are no data on neutron resonances and thus, the information about the level density around B_n in ${}^{56}\text{Fe}$ has to be obtained by different means. In order to do so, we calculate the level density at B_n in ${}^{57}\text{Fe}$ using a back-shifted Fermi-gas expression with the parameterization of von Egidy *et al.* [19], where we apply an additional overall re-normalization factor to match the level density determined from neutron resonance spacings. Then, we use the same level-density formula (including the same re-normalization factor but with the other parameters for ${}^{56}\text{Fe}$) to calculate the level density at B_n in ${}^{56}\text{Fe}$. Using this data point instead of the unknown neutron resonance spacing, we proceed in the same way as for the other three nuclei [1,20].

In Fig. 4 we show the physically most relevant solutions for the level densities in ${}^{56,57}\text{Fe}$ and ${}^{96,97}\text{Mo}$ from the least χ^2 fit. The most striking feature in those curves are the steps starting at 2.9 MeV and 1.8 MeV in ${}^{56}\text{Fe}$ and ${}^{57}\text{Fe}$. There are also less pronounced but still statistically significant step structures at 2.0 MeV and 1.2 MeV in ${}^{96}\text{Mo}$ and ${}^{97}\text{Mo}$. It has been established in the rare-earth region that such low-lying step structures are connected to the breaking of the first nucleon Cooper pair [21]. It is therefore natural to assume that the same is true for the lighter mass regions. The additional step at 6 MeV in the level density curve of ${}^{96}\text{Mo}$ might be due to the opening of the $g_{9/2}$ shell which is indicated to happen at this excitation energy (see Fig. 1). A future systematic investigation of Mo nuclei might shed more light on this issue.

The difference in binding energy between the even and odd systems is a measure for pairing correlation and can be calculated from the three-mass indicator of Dobaczewski *et al.* [22]. This indicator yields 1.2 MeV and 0.9 MeV for the Fe and Mo nuclei, respectively, which agrees very well with the differences in excitation energy for the first steps in the level density curves. Thus we know that the steps in neighboring nuclei appear at the same 'effective' excitation energy, i.e., the excitation energy corrected for the contribution to the binding energy due to neutron-pairing correlations. Further, the average proton pairing energies are 0.8 MeV and 1.1 MeV for the ${}^{57}\text{Fe}$ and ${}^{97}\text{Mo}$ nuclei, respectively. These energies should now correspond to the excitation energies of the steps in the two odd nuclei. However, the steps are delayed in excitation energy by 1.0 MeV and 0.1 MeV for these two

nuclei. This might be explained by the fact that one not only has to invest the energy to break a proton Cooper pair but also at least one of the unpaired protons has to be promoted to the next unoccupied single-particle level. The spacing of those levels can also be calculated using the Dobaczewski three-mass indicator, giving 2.0 MeV and 0.9 MeV in the two cases. Clearly, the higher single particle spacing for the ^{56}Fe nucleus leads to a larger delay in excitation energy for the step structure to appear compared to the ^{97}Mo nucleus, but obviously the exact excitation energy for the steps in the level density curves cannot be estimated from binding energies, since it will depend on the exact location of the Fermi energy within the single-particle level scheme.

Another complication might arise from the effect of seniority non-conserving interactions, which mix configurations of different seniority and smooth out the step structures in the level densities. To investigate this, we have performed a model calculation. In the model we assume a system of eight particles scattered into an equidistant single-particle level scheme with eight doubly-degenerate levels. As residual interactions we consider a pairing interaction and a seniority non-conserving interaction. Thus, the model Hamiltonian is written as

$$\hat{H} = \epsilon \sum_{i=1}^8 i a_i^\dagger a_i - \frac{1}{2} G \sum_{i,j=1}^8 a_i^\dagger a_{\bar{i}}^\dagger a_j a_{\bar{j}} - \frac{1}{2} \kappa \sum_{i,j,k,l=1}^8 W_{ijkl} a_i^\dagger a_j^\dagger a_k a_l, \quad (3)$$

where a^\dagger and a are Fermion creation and annihilation operators and the labels with bars stand for time reversed orbits. The single particle level spacing ϵ , the strength G of the pairing interaction and the strength κ of the seniority non-conserving interaction W are the only macroscopic parameters of the model. This model with good seniority, i.e., the case of $\kappa = 0$ has already been diagonalized in Ref. [23], and the dotted line in Fig. 5 gives the distribution of eigenvalues with excitation energy, i.e., the exact level density of the model. The individual bumps contain mainly levels with the same seniority, thus the step structures in the level density can be explained by the consecutive breaking of nucleon Cooper pairs. However, the experimental data show that in general the steps are much smoother than in such a simple model calculation indicating the need for seniority non-conserving terms in the Hamiltonian.

An important contribution to seniority breaking comes from quadrupole collectivity, which can change rapidly with mass number for the nuclei under study. Strong, residual quadrupole-quadrupole interactions can lead to deformation of the nucleus and to a modification of the single-particle level spacing. Unfortunately, our simple model cannot incorporate a realistic quadrupole-quadrupole interaction; the smoothing of the level density, however, should not depend on the details of the

seniority non-conserving residual interaction. We choose therefore to model the quadrupole-quadrupole interaction by a random two-body interaction [24] of roughly equivalent strength where all the pairing-like terms have been set to zero i.e., the W_{ijkl} in Eq. (3) are Gaussian random numbers of mean zero and width equal to one except for the cases of $j = \bar{i}$ and $k = \bar{l}$ where $W_{i\bar{i}l\bar{l}} = 0$.

Since in this more general case Eq. (3) does not have good seniority, exact diagonalization of the model Hamiltonian has to be performed within the full model space which is computationally very demanding, as one requires *all* levels, not just the lowest. For eight particles in eight doubly-degenerate states there are 12870 states (counting all magnetic substates). The number of levels (not counting magnetic substates) equals the number of states with spin projection $J_z = 0$, thus yielding 4900 levels. For the present calculations, we used $\epsilon = 0.25$ MeV, $G = 0.5$ MeV, and $\kappa \approx 0$ MeV (pure pairing) and $\kappa = 0.14$ MeV (pairing+random interaction). In Fig. 5, we show the resulting level densities of the two calculations. The resolved bumps with definite seniority in the pure pairing case are smeared out by the random interaction. The gaps between the bumps are rapidly being filled, while the bumps themselves are degraded into a step structure quite similar to the step structure seen in the experimental level density curves of the iron nuclei. The occurrence of the step structure in the calculation is actually quite sensitive to the exact choice of the strength of the random interaction. A weak random interaction ($\kappa < 0.1$ MeV) does not fill the gaps between the bumps, a strong random interaction ($\kappa \geq 0.2$ MeV) produces a more smeared out step structure in the level density curve similar to the Mo data, indicating the presence of relatively stronger seniority non-conserving interactions in the Mo nuclei. The range of values which produces good qualitative agreement with the Fe data is about $0.13 \text{ MeV} \leq \kappa \leq 0.16 \text{ MeV}$. However, due to the simplicity of the model, no attempt has been made to achieve quantitative agreement between the model and the experimental data.

In conclusion, we have presented new experimental data on level densities below B_n in $^{56,57}\text{Fe}$ and $^{96,97}\text{Mo}$. Step structures in the level density curves have been related to the breaking of nucleon Cooper pairs. The occurrence of the step structures in energy depends on the exact location of the Fermi energy in the single particle level scheme. The smoothness of the step structures depends on the strength of the seniority non-conserving interactions, e.g., the quadrupole-quadrupole interaction compared to the pairing interaction and the average single-particle level spacing. The more pronounced step structures in the level density data of Fe nuclei compared to Mo indicate relatively stronger seniority non-conserving interactions in the latter case. Our schematic calculations where random two-body interactions were used to model residual seniority non-conserving interactions show that level density curves are very sensitive to the relative strengths of the different terms in the model

Hamiltonian. The present experimental data therefore break new ground for the possible theoretical investigation of two of the most important residual interactions in atomic nuclei, namely the pairing and the quadrupole-quadrupole interaction

Part of this work was performed under the auspices of the U.S. Department of Energy by the University of California, Lawrence Livermore National Laboratory under Contract No. W-7405-ENG-48. Financial support from the Norwegian Research Council (NFR) is gratefully acknowledged. G.M. acknowledges support by a U.S. Department of Energy grant with No. DE-FG02-97-ER41042.

-
- [1] A. Schiller, L. Bergholt, M. Guttormsen, E. Melby, J. Rekstad, and S. Siem, Nucl. Instrum. Methods Phys. Res. A **447**, 498 (2000).
- [2] G. A. Bartholomew, I. Bergqvist, E. D. Earle, and A. J. Ferguson, Can. J. Phys. **48**, 687 (1970).
- [3] G. A. Bartholomew, E. D. Earle, A. J. Ferguson, J. W. Knowles, and M. A. Lone, Adv. Nucl. Phys. **7**, 229 (1973).
- [4] A. Schiller, A. Bjerve, M. Guttormsen, M. Hjorth-Jensen, F. Ingebretsen, E. Melby, S. Messelt, J. Rekstad, S. Siem, and S. W. Ødegård, Phys. Rev. C **63**, 021306(R) (2001).
- [5] E. Melby, M. Guttormsen, J. Rekstad, A. Schiller, S. Siem, and A. Voinov, Phys. Rev. C **63**, 044309 (2001).
- [6] A. Voinov, M. Guttormsen, E. Melby, J. Rekstad, A. Schiller, and S. Siem, Phys. Rev. C **63**, 044313 (2001).
- [7] S. Siem, M. Guttormsen, K. Ingeberg, E. Melby, J. Rekstad, A. Schiller, and A. Voinov, Phys. Rev. C **65**, 044318 (2002).
- [8] M. Guttormsen, E. Melby, J. Rekstad, S. Siem, A. Schiller, T. Lönnroth, and A. Voinov, J. Phys. G **29**, 263 (2003).
- [9] E. Margaret Burbridge, G.R. Burbridge, William A. Fowler, and F. Hoyle, Rev. Mod. Phys. **29**, 547 (1957).
- [10] George Wallenstein *et al.*, Rev. Mod. Phys. **69**, 995 (1997).
- [11] S. I. Al-Quraishi, S. M. Grimes, T. N. Massey, and D. A. Resler, Phys. Rev. C **63**, 065803 (2001).
- [12] W. Hauser and H. Feshbach, Phys. Rev. **87**, 366 (1952).
- [13] M. Guttormsen, A. Atac, G. Løvhøiden, S. Messelt, T. Ramsøy, J. Rekstad, T. F. Thorsteinsen, T. S. Tveter, and Z. Zelazny, Phys. Scr. **T32**, 54 (1990).
- [14] S. Cochavi, A. Moalem, D. Ashery, J. Alster, G. Bruge, and A. Chaumeaux, Nucl. Phys. **A211**, 21 (1973).
- [15] M. Guttormsen, T. S. Tveter, L. Bergholt, F. Ingebretsen, and J. Rekstad, Nucl. Instrum. Methods Phys. Res. A **374**, 371 (1996).
- [16] M. Guttormsen, T. Ramsøy, and J. Rekstad, Nucl. Instrum. Methods Phys. Res. A **255**, 518 (1987).
- [17] D. M. Brink, Ph.D. thesis, Oxford University, 1955.
- [18] P. Axel, Phys. Rev. **126**, 671 (1962).
- [19] T. von Egidy, H. H. Schmidt, and A. N. Bekhami, Nucl. Phys. **A481**, 189 (1988).
- [20] E. Tavukcu, Ph.D. thesis, North Carolina State University, 2002.
- [21] E. Melby, L. Bergholt, M. Guttormsen, M. Hjorth-Jensen, F. Ingebretsen, S. Messelt, J. Rekstad, A. Schiller, S. Siem, and S. W. Ødegård, Phys. Rev. Lett. **83**, 3150 (1999).
- [22] J. Dobaczewski, P. Magierski, W. Nazarewicz, W. Satuła, and Z. Szymański, Phys. Rev. C **63**, 024308 (2001).
- [23] M. Guttormsen, A. Bjerve, M. Hjorth-Jensen, E. Melby, J. Rekstad, A. Schiller, S. Siem, and A. Belić, Phys. Rev. C **62**, 024306 (2000).
- [24] K.K. Mon and J.B. French, Ann. Phys. (N.Y.) **95**, 90 (1975).

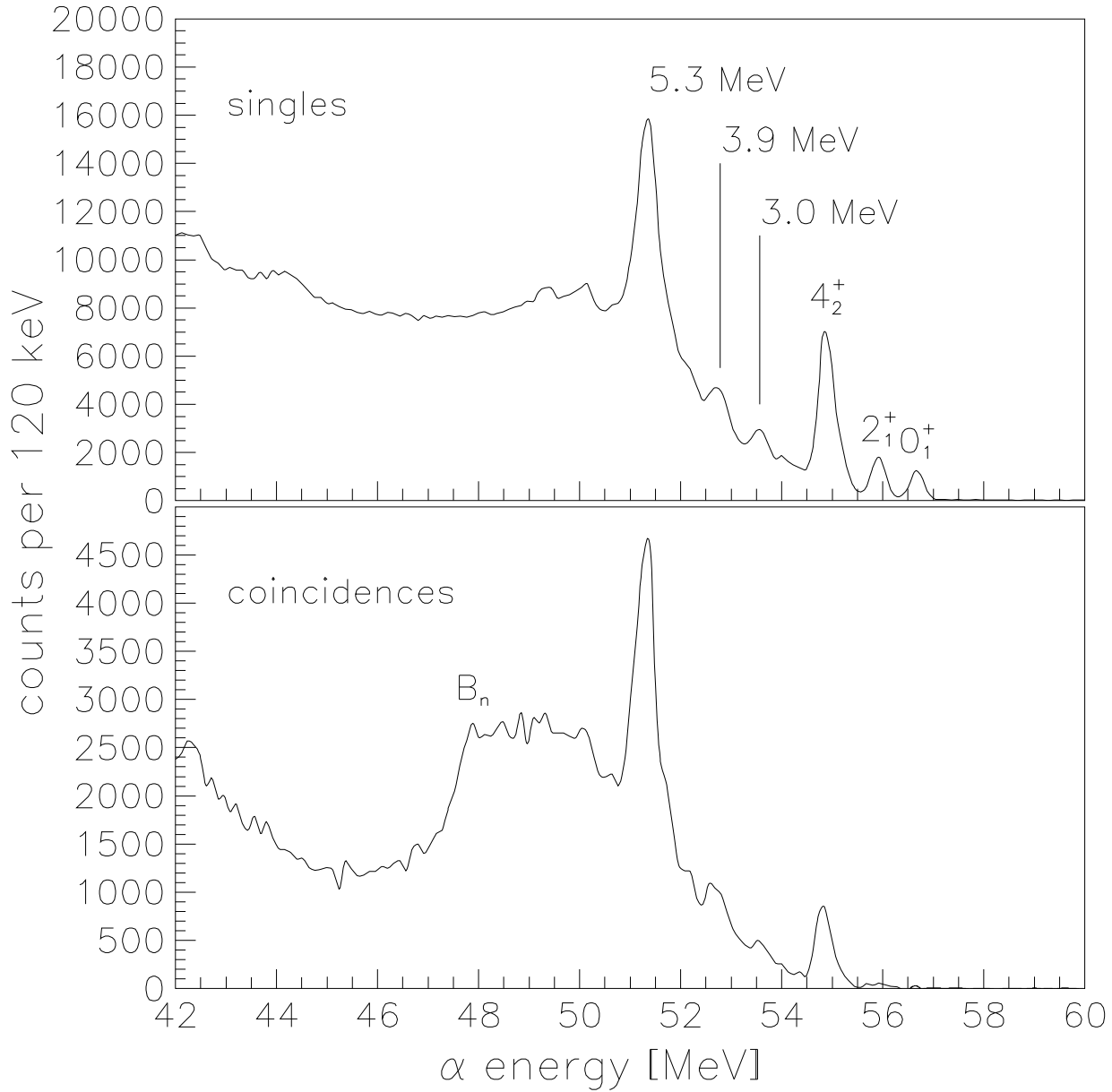


FIG. 1. A singles α spectra is shown in the upper panel and an α - γ coincidence spectrum is shown in the lower panel for the $^{97}\text{Mo}(^3\text{He},\alpha)^{96}\text{Mo}$ reaction. At the neutron binding energy B_n , the coincidence spectrum shows a dip reflecting the lower γ multiplicity in the decay from low-lying states in ^{95}Mo which are populated by neutron emission. The transfer peaks to the first three states are well known from the (p,d) reaction [14]. The strong transfer peak at 5.3 MeV is a new discovery and indicates the opening of the neutron $g9/2$ shell at this energy.

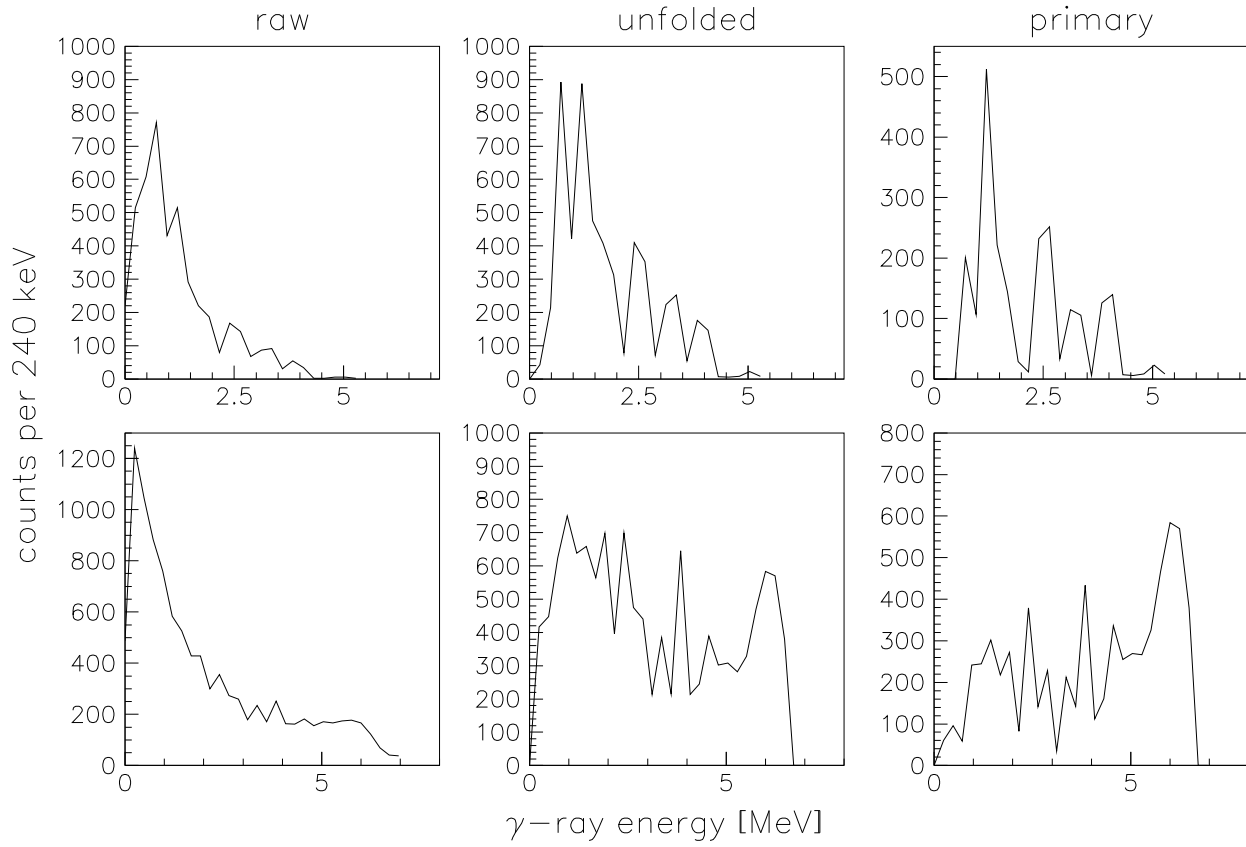


FIG. 2. Raw, unfolded, and primary γ spectra from the $^{57}\text{Fe}(^3\text{He},\alpha\gamma)^{56}\text{Fe}$ reaction at 5 MeV excitation energy (upper panels) and from the $^{57}\text{Fe}(^3\text{He},^3\text{He}'\gamma)^{57}\text{Fe}$ reaction at 6.2 MeV excitation energy (lower panels).

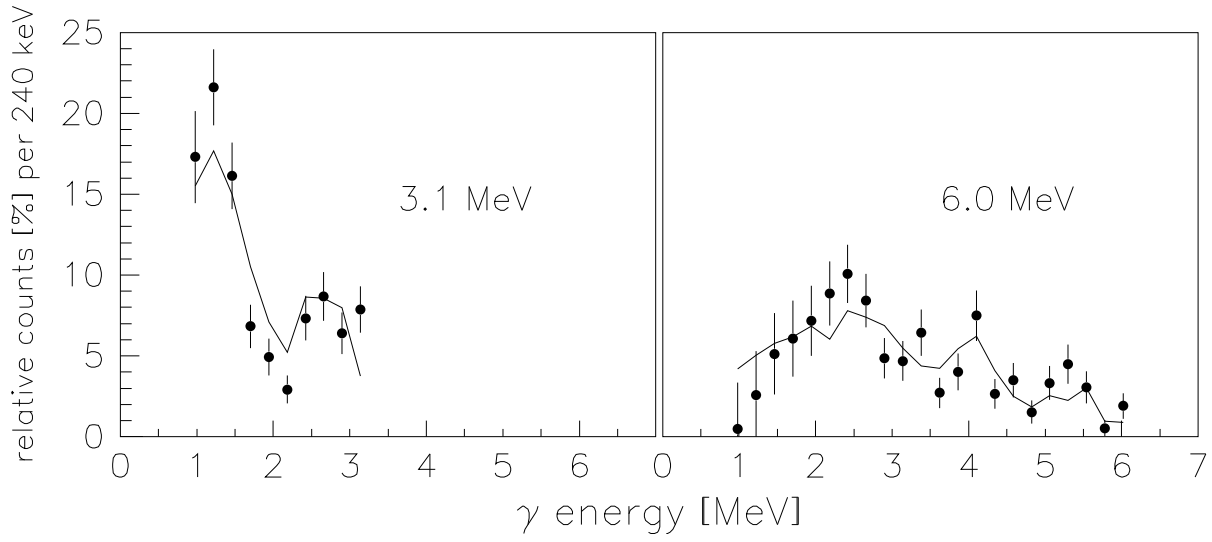


FIG. 3. Experimental primary γ spectra (data points with error bars) at two different initial excitation energies (indicated in the figure) compared to the least χ^2 fit (solid lines) for the $^{97}\text{Mo}({}^3\text{He}, {}^3\text{He}'\gamma)^{97}\text{Mo}$ reaction. The fit is performed simultaneously to the whole primary γ matrix of which the two displayed spectra are only a small fraction. The first generation spectra are normalized to one at each excitation energy.

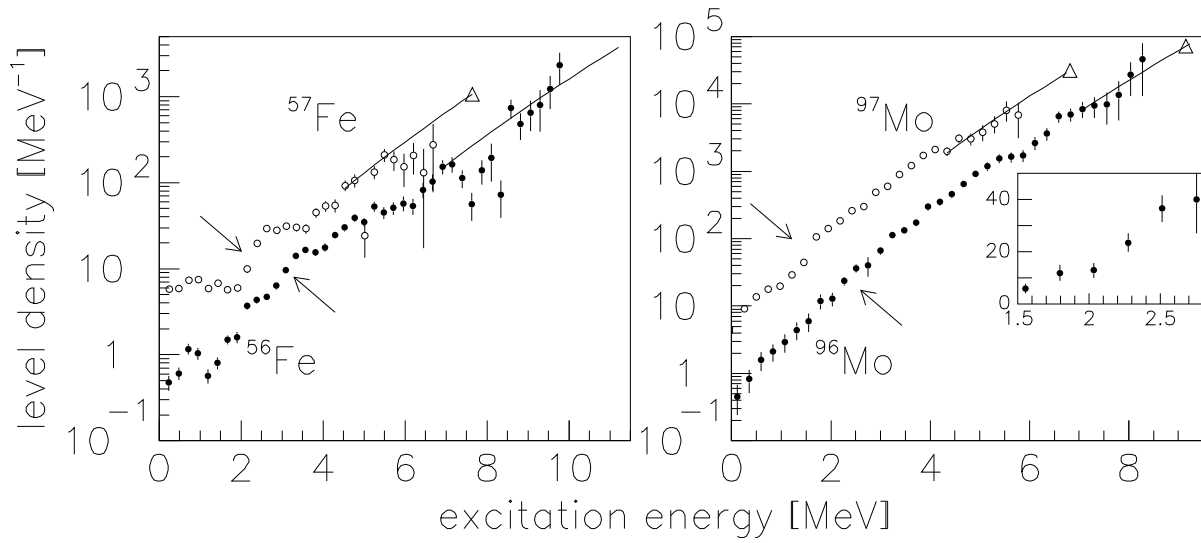


FIG. 4. Experimental level densities for the four nuclei under study. Where available, level density data from neutron resonance spacings have been added (open triangles). The solid lines are the re-normalized level density parameterizations according to von Egidy *et al.* [19]. Step structures in the level densities are marked by arrows. The insert shows the step structure for ⁹⁶Mo on a linear scale. In the level density of ⁵⁶Fe, the bump and the plateau at 0.8 MeV and 2.0 MeV, respectively, are due to the first and second excited states.

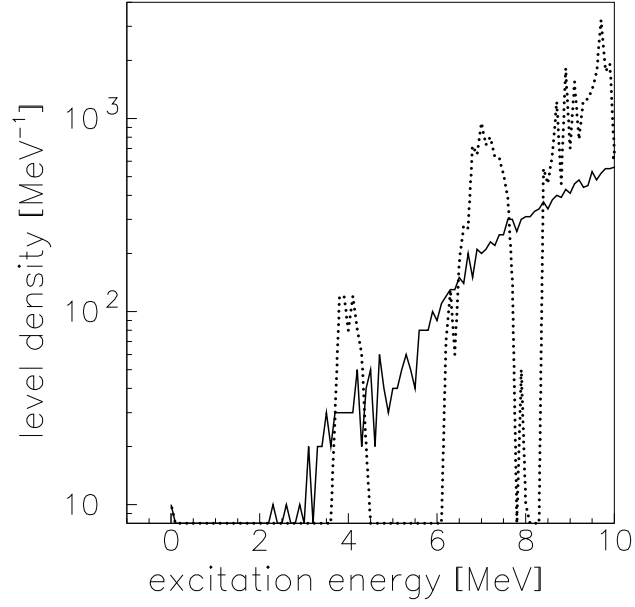


FIG. 5. Model calculation using the Hamiltonian of Eq. (3) with $\epsilon = 0.25$ MeV, $G = 0.5$ MeV, and $\kappa = 0$ MeV (dotted line). The level density is given as function of excitation energy. Adding a random two-body interaction with the strength $\kappa = 0.14$ MeV (solid line) results in a step structure quite similar to what is seen in the experimental level density curve of the iron nuclei.